THE ASTROPHYSICAL JOURNAL, 285:527–546, 1984 October 15


# EXTENDED GASEOUS EMISSION IN NORMAL ELLIPTICAL GALAXIES[1]

M.-H. DEMOULIN-ULRICH[2]
European Southern Observatory
H. R. BUTCHER
Kapteyn Astronomical Institute, University of Groningen
AND
A. BOKSENBERG
Royal Greenwich Observatory
*Received 1983 September 6; accepted 1984 March 29*

## ABSTRACT

We report observations of the spatial distribution, the velocity field, and the line intensities of the extended gaseous emission in a small sample of nearby normal elliptical galaxies. Ionized gas regions extending 1–3 kpc in diameter are found in six out of 12 ellipticals selected for having gas in their nuclei. Extended gaseous emission is therefore not an uncommon phenomenon. The velocity field of the gas is in every case consistent with the gas being in a disk in rotation around the nucleus, but turbulent motions are dominant in the center as evidenced by the increase in the line width near the nucleus. Among the galaxies where we could determine the axis of rotation of the gas there is no clear correlation between the position angle of that axis and the position angle of the rotation axis or of the minor axis of the stellar population. In NGC 4278, the best studied case, it is found that the position angle of the rotation axis of the ionized gas differs from that of the neutral gas and of the stellar population. This can be explained by differential precession of the gas with the ionized gas being closer to settling in the equatorial plane than is the neutral gas which is located further out. It is also consistent with the ionized and neutral gas moving along the normal elliptic orbits in the equatorial plane of a triaxial ellipsoid.

Considerations regarding the total energy necessary to keep the gas ionized allow the identification of likely and unlikely sources of energy responsible for keeping the gas ionized. These considerations, however, include parameters which are not well determined such as the efficiency of the conversion of kinetic energy into H$\beta$ photons through shocks, or the filling factor of the gas. It is found that in galaxies where the equivalent width of H$\beta$ is more than $\sim$0.1 Å, the ultraviolet stellar photons, the stellar winds, and the supernovae ejecta are probably insufficient to ionize the gas. In galaxies where the equivalent width of H$\beta$ is larger than $\sim$5 Å, the gas shed by the stars and falling on the central disk of ionized gas does not provide enough energy to keep the gas ionized. The only possible sources of the ionization in this case appear to be either a central non-thermal source or the accretion energy of gas captured from outside the galaxy. The present state of the observations and of the models does not permit the distinction between these two possibilities.

*Subject headings:* galaxies: internal motions — galaxies: nuclei — galaxies: structure — interstellar: matter

## I. INTRODUCTION

Direct evidence regarding the origin of the gas which is observed to be present in elliptical galaxies can be obtained from the dynamics and the elemental abundances of the gas. There are two possibilities for the origin of the gas. One is that it is a part of the gas shed by evolving stars in the galaxy. The rate of mass loss from a population typical of an elliptical galaxy and emitting $10^9\ L_\odot$ is estimated to be 0.015 $M_\odot$ per year (Faber and Gallagher 1976) which corresponds to a total mass of $10^9$–$10^{10}\ M_\odot$ of gas produced in $10^{10}$ yr by the stars in an elliptical galaxy of luminosity $10^{10}\ L_\odot$. In contrast, the mass of ionized gas which is observed in normal elliptical galaxies is usually less than $10^7\ M_\odot$. Similarly, except for a few objects, the upper limits to the mass of neutral hydrogen gas in ellipticals are about $10^7$–$10^8\ M_\odot$ (e.g., Sancisi 1981). The discrepancy between the amount of gas produced by the stars and the upper limits to the mass of neutral and ionized gas led Mathews and Baker (1971) to propose a model of a galactic wind which would sweep the gas out of the galaxy. If this sweeping mechanism is not completely efficient or if it is not turned on all the time some fraction of the gas would remain in the galaxy (Mathews and Baker 1971; Sanders 1981). Its kinematics is determined by the gravitational potential of the stars, and its elemental abundance should be the same as that of the evolved stars in the galaxy, at least as metal rich as the Sun.

Alternatively, in at least some cases, the gas presently located in an elliptical galaxy could have come from outside the galaxy, either by being accreted from the outer regions of a nearby spiral or through the merger of the elliptical and of a gas-rich system (isolated H I clouds if such objects exist, or a Magellanic-type galaxy). In this case the gas is expected to be metal poor and its dynamics to remain strongly influenced by its initial angular momentum. Eventually, the gas settles in one of the principal planes of the elliptical galaxy. This process is now being investigated by a number of authors (van Albada,

[1] Based on observations collected at the European Southern Observatory and at Kitt Peak National Observatory; Kitt Peak National Observatory is operated by the Association of Universities for Research in Astronomy, Inc., under contract with the National Science Foundation.
[2] Visiting Astronomer, Kitt Peak National Observatory.

Kotanyi, and Schwarzschild 1982; Tohline and Durisen 1982; Heisler, Merritt, and Schwarzschild 1982).

In an effort to distinguish between the possible origins for the gas, and the different ionization mechanisms, we have observed some of the nearest normal ellipticals known to have ionized gas and have obtained the maps and the velocity field of the extended ionized regions as well as some spectrophotometric data on the gas in the nucleus.

## II. OBSERVATIONS

We observed the nearest galaxies reported to be ellipticals with emission lines in the survey of Humason, Mayall, and Sandage (1956). Since the time of this survey better direct photographs have become available and have allowed the making of a more accurate determination of the morphological type (Sandage and Tammann 1981). Some basic data on the galaxies observed are listed in Table 1, columns (2)–(4).

### *a) Imaging the Ionized Gas*

Digital images through narrow-band filters were first secured with the KPNO video camera digital television system at the Mayall 4 m telescope. One filter for each object was 50 Å wide and centered in wavelength to pass the light of Hα + [N II] λλ6548, 6583 at the redshift of the galaxy. The other filter was centered at 6200 Å and had a width of 175 Å. This latter filter provided an off-band or continuum observation to be used to remove the background starlight of the object. Integration times for each object and filter combination were either 13 or 27 minutes. After dark subtraction and flat fielding (cf. Ford and Butcher 1979), all frames were corrected for distortion using third-order interpolation and including terms up to fifth order in both the radial and the tangential directions. The resulting frames cover just over 1′ of sky and have a scale of 0.″29 per pixel.

In the next step in generating the emission-line maps of interest, the off-band frame for each object was shifted spatially to align it with the on-band image. Linear interpolation was used in this step, which has the effect of gently smoothing the off-band data; because the seeing is well sampled, no degradation in net resolution is incurred by this operation. Alignment accuracies of ±0.″01 were found to be readily attainable on these bright, centrally condensed galaxies; accuracies of ±0.″03 or so are required to prevent the appearance of "derivative" features near the centers. In no case were the extended emission-line regions visible in the raw on-band frames, so it seems unlikely that they are ever bright enough in these galaxies to bias the spatial alignment of the frames.

To actually produce the required maps, the aligned off-band frame was next scaled in flux to match the on-band data and subtracted from those data. This scaling procedure has proved the weak link in the whole process. Scaling accuracies of 1% or so are required, but problems associated with the wavelength differences of the filters, which introduce color dependence, with the sky level determination, and with transparency variations between the frames, all make accuracies of this order hard to achieve. Consequently, our solution was to produce a series of subtractions, with a sequence of scaling ratios centered on an estimated value. For off-band–to–on-band ratios which are too large, rings of negative data appear in the subtracted frame; for ratios which are too small, concentric gradients of apparent emission appear. The series of subtracted frames was examined visually on a TV monitor, and the "best" ratio selected as the final map.

Note that this method produces results which are insensitive to the presence of line-emitting material distributed like the background starlight. However, comparison of our long-slit spectra (§ IV) with our emission-line maps shows that such emission is rarely, if ever, present. That is, our spectra show the maps to be faithful to within the noise along those position angles sampled.

Final contour maps were generated by scaling all data to a uniform flux scale and by smoothing each map to yield a point spread function of 2.″0 FWHM. Our final data for the different objects then should be closely comparable in quality.

TABLE 1

CHARACTERISTICS OF THE EXTENDED IONIZED REGION

| | | | | Extended Emission | | | |
|---|---|---|---|---|---|---|---|
| NGC (1) | Type (2) | $M_{B_T}$ (3) | Distance (Mpc) (4) | Outer Isophotes (arcsec) (5) | P.A. Major Axis (6) | P.A. Kinematic Major Axis (7) | P.A. Major Axis Stellar Isophotes (8) |
| 2974 ..... | E4 | −21.12 | 36 | 6 × 6 | circular | 45 ± 10 | 45 |
| 3156 ..... | E5: | −18.50 | 20 | ... | ... | ... | ... |
| 3226 ..... | S01 | −19.71 | 25 | ... | ... | ... | ... |
| 3773 ..... | pec. jet | −18.2 | 17 | 8 × 8 | circular | (c)a | ... |
| 3904 ..... | E2 | −20.30 | 27 | ... | ... | ... | ... |
| 3962 ..... | E1 | −20.89 | 32 | 10 × 7 | 35 | 88 ± 10 | 0 |
| 4278 ..... | E1 | −19.24 | 16.4[b] | 25 × 10 | 63 | 40 ± 12 | 20 |
| 4636 ..... | E0/S0 | −20.58 | 16 | 20 × 20 | complex | [c] | 152[d] |
| 5077 ..... | E3 | −21.03 | 51 | 15 × 12 | 90? | 83 ± 15 | 5 |
| 5444 ..... | E3 | −22.01 | 80 | ... | ... | ... | ... |
| 5846 ..... | S01(0) | −21.49 | 33 | 15 × 15 | complex | 90 ± 10 | 64[d] |
| 3C 317 ..... | E | −21.38 | 210[e] | 12 × 12 | complex | [c] | 25 |

NOTE.—$H = 50$ km s$^{-1}$ Mpc$^{-1}$.

[a] Velocity gradient is less than 30 km s$^{-1}$ per 10″.

[b] Distance from Raimond *et al.* 1981.

[c] Velocities were measured in one P.A.

[d] From King 1978.

[e] Type, magnitude, and distance of 3C 317 are from Sandage, Kristian, and Westphal 1976.

*b) Measuring the Velocity Field of the Ionized Gas*

The spectroscopic observations were made in 1979 and 1980 with the Image Photon Counting System (IPCS) of the University College London (Boksenberg 1978) attached to the Cassegrain spectrograph of the 3.6 m ESO telescope. The average seeing was 2″. The galaxies were observed in several position angles across the nucleus with usually two spectra in each position angle, one in the range 3600–4500 Å with a resolution of 1.6 Å and another in the range 5800–7600 Å with a resolution of 3.2 Å. Spectra of the blank sky were recorded separately. These data were supplemented by some lower dispersion spectra covering the range 3600–7000 Å. The 1979 data were recorded in an array of 72 lines or increments of 1500 spectral elements, with each increment covering 1″.7 on the sky. In 1980 the frame format was 84 lines by 1500 spectral elements, and each increment represented 2″.18 on the sky. See Table 2.

With this spectrographic material it is possible to measure the velocities of the ionized gas with adequate accuracy (see § IV) below) whenever the equivalent width of the emission lines which are measured is larger than 4 Å. The equivalent width of Hα and [N II] λ6584 dropped below this value within a few arc seconds from the nucleus, and therefore the velocities outside the central regions all come from the (unresolved) doublet [O II] λ3727.

TABLE 2

SPECTROSCOPIC OBSERVATIONS

| NGC | Position Angle (deg.) | Exposure (s) | Spectral Range[a] |
|---|---|---|---|
| 2974 ..... | 45 | 4940 | 2 |
| | 135 | 3000 | 3 |
| 3773 ..... | 0 | 210 | 2 |
| | 90 | 400 | 2 |
| 3962 ..... | 6 | 1000 | 1 |
| | 6 | 1500 | 2 |
| | 66 | 1000 | 1 |
| | 66 | 2900 | 2 |
| | 96 | 1000 | 1 |
| | 96 | 1500 | 2 |
| | 170 | 1650 | 3 |
| 4278 ..... | 25 | 2000 | 1 |
| | 25 | 2500 | 2 |
| | 63 | 1600 | 1 |
| | 63 | 2500 | 2 |
| | 153 | 1300 | 1 |
| | 153 | 500 | 2 |
| | 0 | 6037 | 3 |
| | 0 | 1860 | 2 |
| | 63 | 4000 | 3 |
| | 108 | 2025 | 1 |
| | 108 | 1520 | 2 |
| 4636 ..... | 0 | 3005 | 3 |
| 5077 ..... | 66 | 1200 | 1 |
| | 66 | 1200 | 2 |
| | 90 | 3760 | 1 |
| | 90 | 1000 | 2 |
| | 118 | 1500 | 1 |
| | 118 | 1000 | 2 |
| | 66 | 4400 | 3 |
| 5846 ..... | 0 | 2916 | 1 |
| | 90 | 2650 | 1 |
| 3C 317 ..... | 0 | 1500 | 3 |

[a] Spectral ranges. 1: 3600–4500 Å; 2: 5800–7600 Å; 3: 3600–7200 Å.

To extend the measurements as far away from the nucleus as possible, adjacent increments were added to augment the signal-to-noise ratio (at the expense of spatial resolution).

## III. THE DISTRIBUTION OF THE IONIZED GAS

We have found an extended region of ionized gas of typically 2 kpc in diameter in eight ellipticals out of the 13 which we observed with the Video Camera. In the other galaxies which were observed gas is detected in the nucleus only. From this limited sample it thus appears that the presence of *extended* emission is not a rare phenomenon among elliptical galaxies which have emission lines in their optical spectrum.

The Hα + [N II] λ6584 maps for seven ellipticals with extended emission are presented in Figures 1–7 together with portions of the Palomar Sky Survey E plates showing the orientation of the outer isophotes of the stellar component of each galaxy and the presence or absence of nearby neighbors. The contours in the emission line maps are in steps of $4.0 \times 10^{-15}$ ergs cm$^{-2}$ s$^{-1}$. Extended emission is also detected in NGC 3773 which turned out to be a small gas-rich galaxy and in the radio galaxy 3C 317, the brightest member of the cluster A2052. In both galaxies the extended emission is a few arc seconds in diameter and appears circular.

The dimensions and orientation of the ionized gas regions are given in Table 1, columns (5) and (6), and the position angles of the major axis of the outer stellar isophotes are given in column (8).

The surface brightness of the extended emission is always maximum at the nucleus (except in NGC 4636), and it is more sharply peaked than is the stellar population.

The outer isophotes of the extended emission region typically occur at radii less than about $\frac{1}{2}R_e$, the de Vaucouleurs effective (half-light) radius, and have a variety of shapes. Only in two cases, NGC 3962 and NGC 4278, do they clearly show an elongated contour approximating an ellipse with the nucleus at the center. In neither of these cases is the major axis of the gaseous region aligned with the major or the minor axis of the stellar population. In NGC 2974, an E5 elliptical, and NGC 5077, an E3 elliptical, the outer isophotes are approximately circular, while in NGC 4636 and NGC 5846 they have an irregular shape and are asymmetrical with respect to the nucleus. There is no case where the ionized gas distribution resembles a thin disk of gas seen edge on. This together with the increase of the velocity dispersion of the gas near the nucleus (§ IV) indicates that, very close to the center, the gas is most likely not settled in one of the principal planes of the galaxy and that its motion is mostly turbulent.

Regarding the effect of the environment, we note that gas is present in ellipticals located in tight groups such as NGC 4278, NGC 5077, and NGC 5846 as well as in galaxies which appear isolated like NGC 2974, NGC 3962, and NGC 4636. In that respect it would be of interest to search the surroundings of NGC 2974 and NGC 3962, the two isolated galaxies with the most intense lines in our sample, for the presence of gas-rich small systems either by observing in 21 cm or by taking deep photographs in the 4000–5000 Å range.

NGC 4278 is the only elliptical in our observing list which has been mapped at 21 cm. The distribution of the neutral gas is consistent with the gas being in an oval ring with an inclination of ~45° on the line of sight (Raimond *et al.* 1981). The ionized gas is seen interior to the H I ring. The outer contours of the ionized gas roughly form an ellipse with an axis ratio of

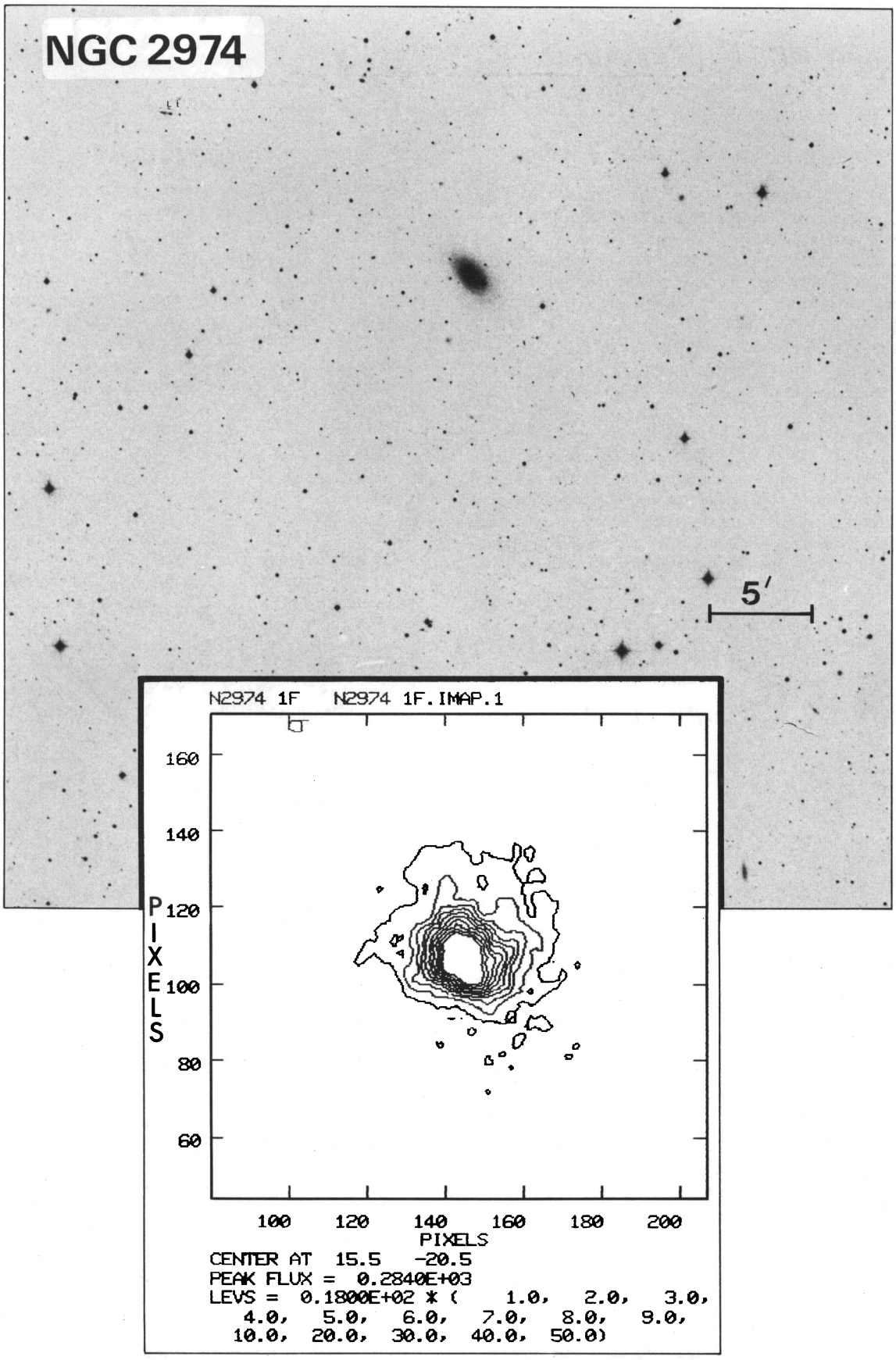


FIG. 1.—(*top*) Portion of the Palomar Observatory Sky Survey E print showing the vicinity of NGC 2974 and the outer contours of the stellar isophotes. (*bottom*) Map of the ionized gas in the Hα + N II emission, obtained with the Video Camera at KPNO. The tick marks are 5″.8 apart. North is up and east to the left.

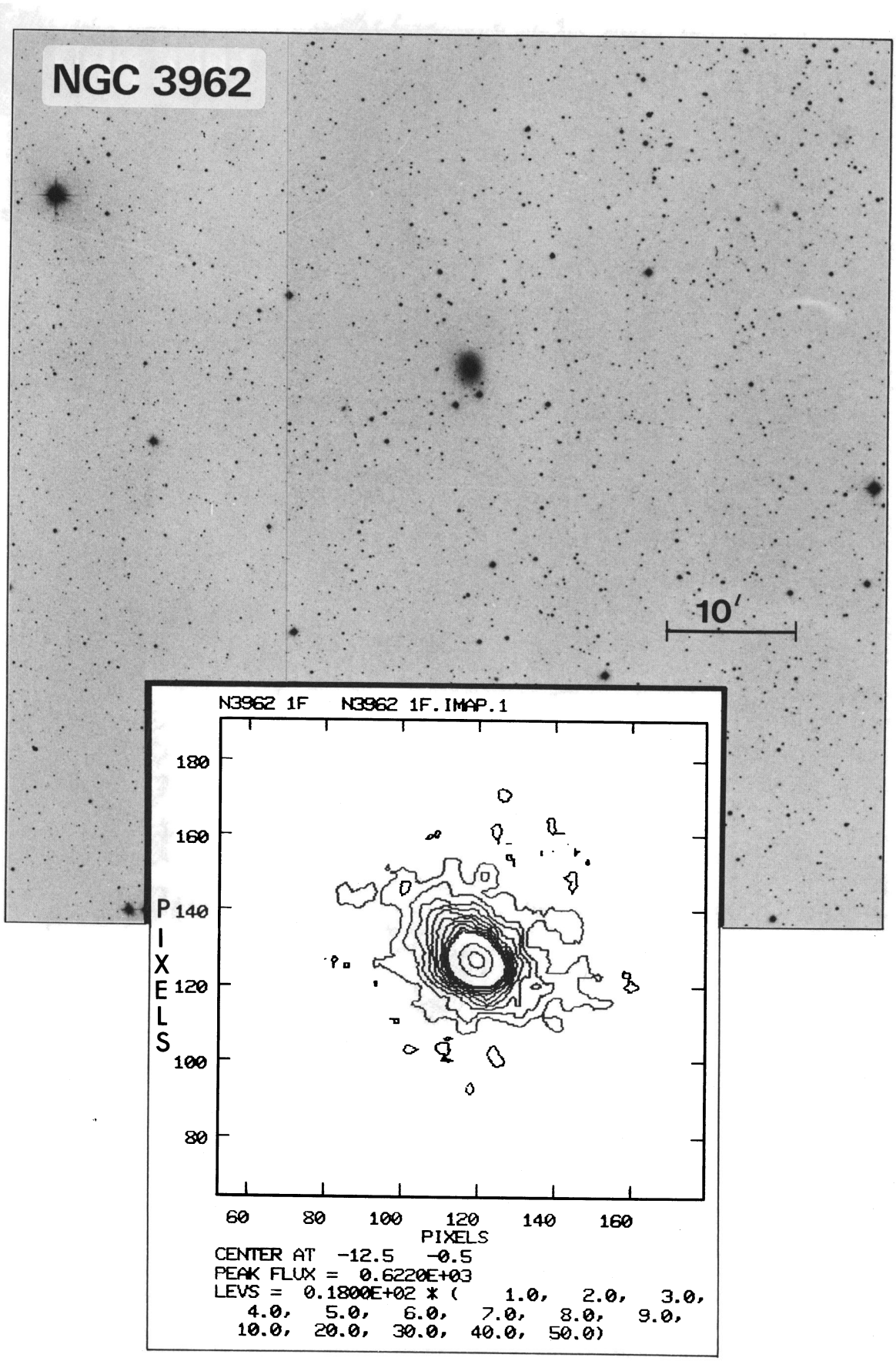


FIG. 2.—Same as Fig. 1 for NGC 3962. 10″ = 1.5 kpc.

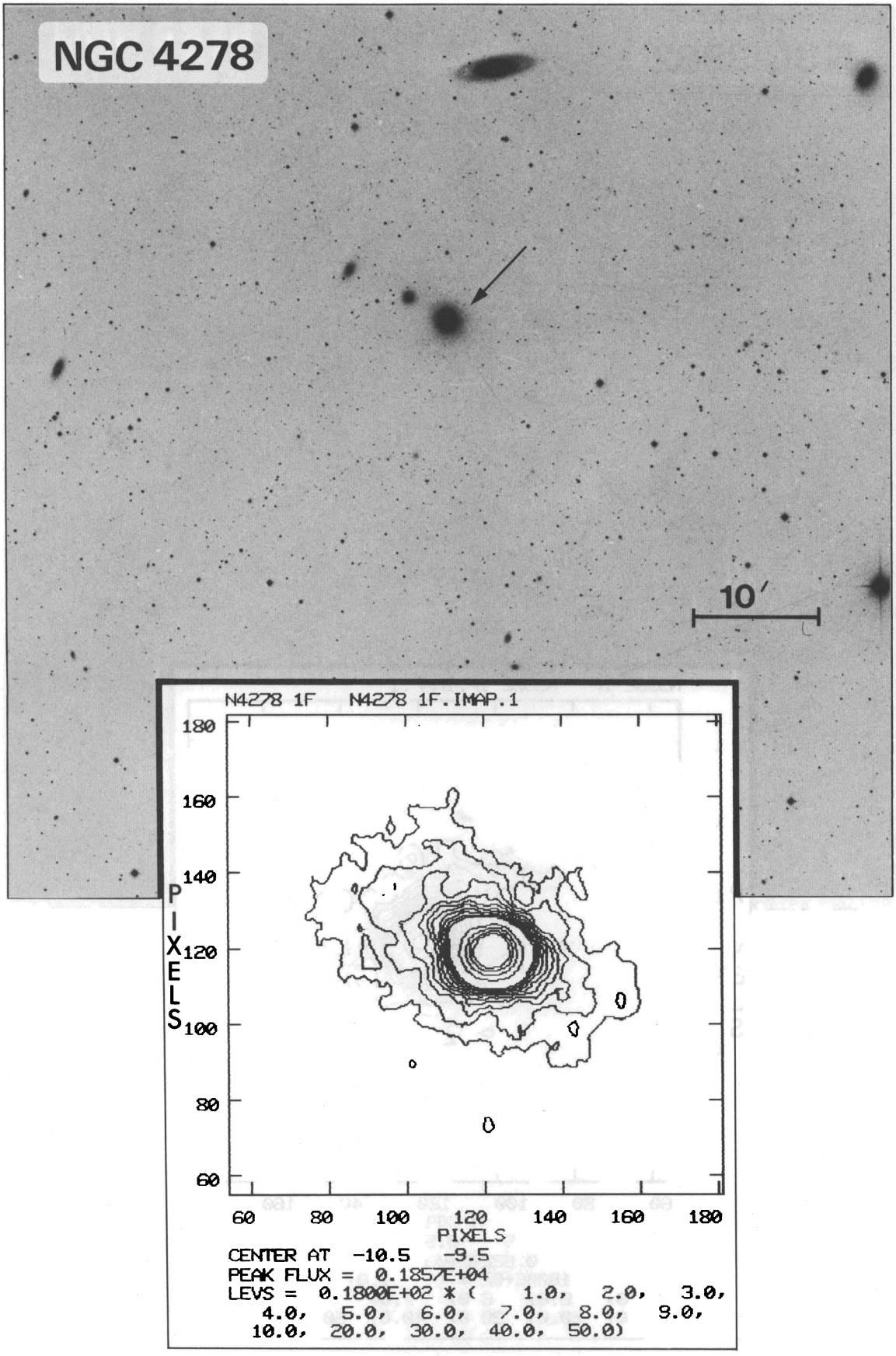


FIG. 3.—Same as Fig. 1 for NGC 4278. 10″ = 800 kpc.

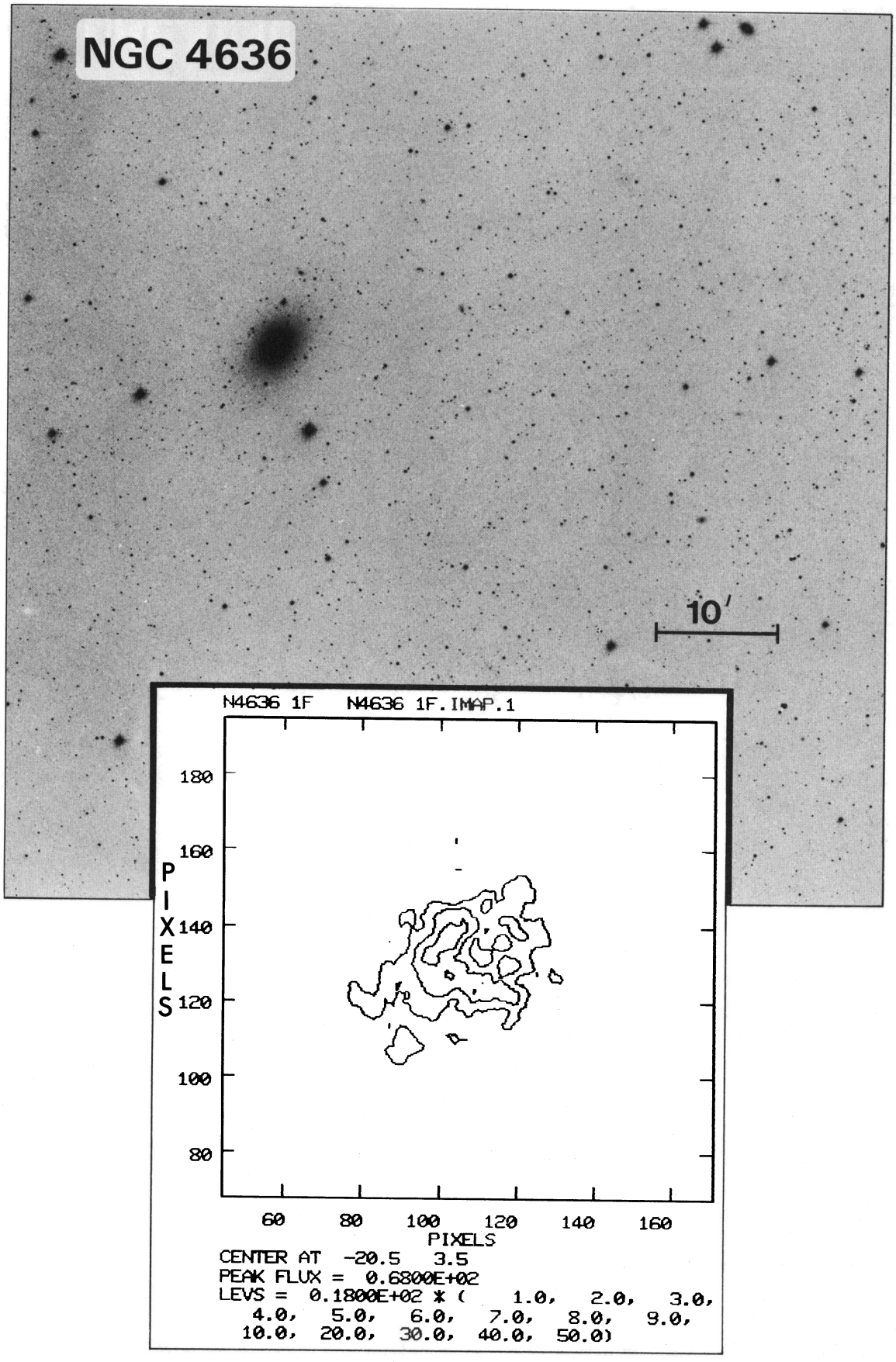


FIG. 4.—Same as Fig. 1 for NGC 4636. 10″ = 800 kpc.

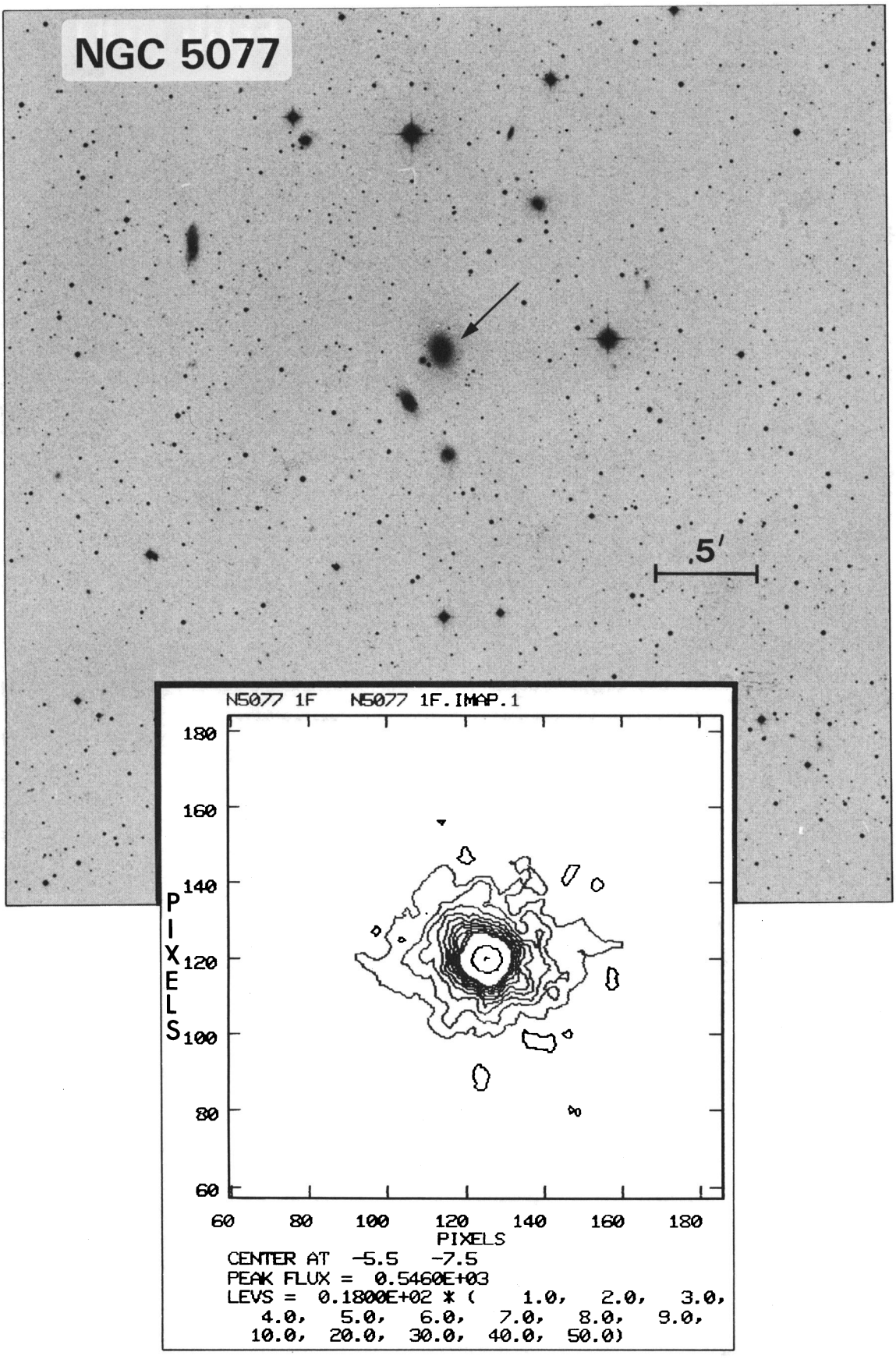


FIG. 5.—Same as Fig. 1 for NGC 5077. 10″ = 2.5 kpc.

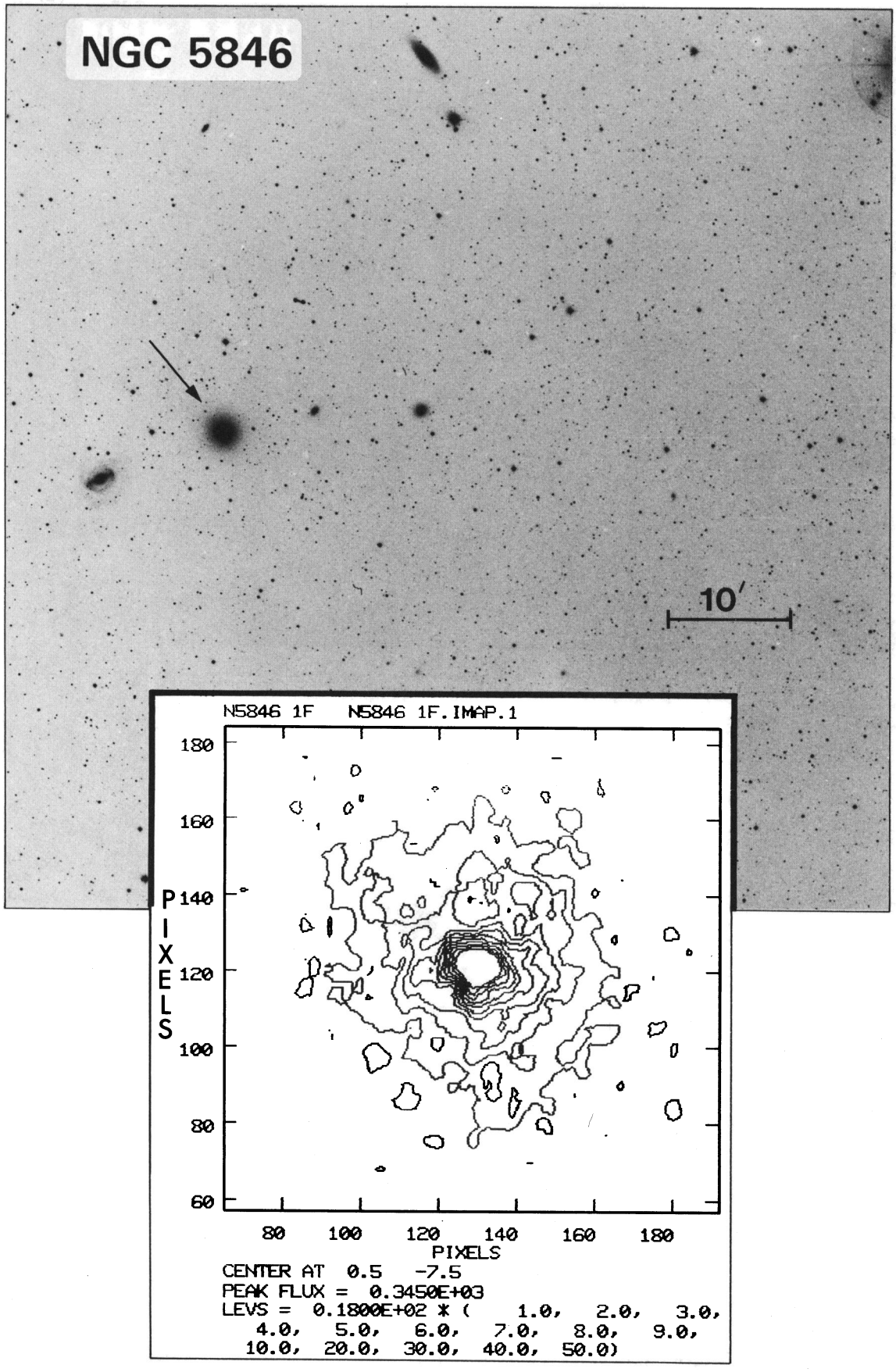


FIG. 6.—Same as Fig. 1 for NGC 5846. 10″ = 1.6 kpc.

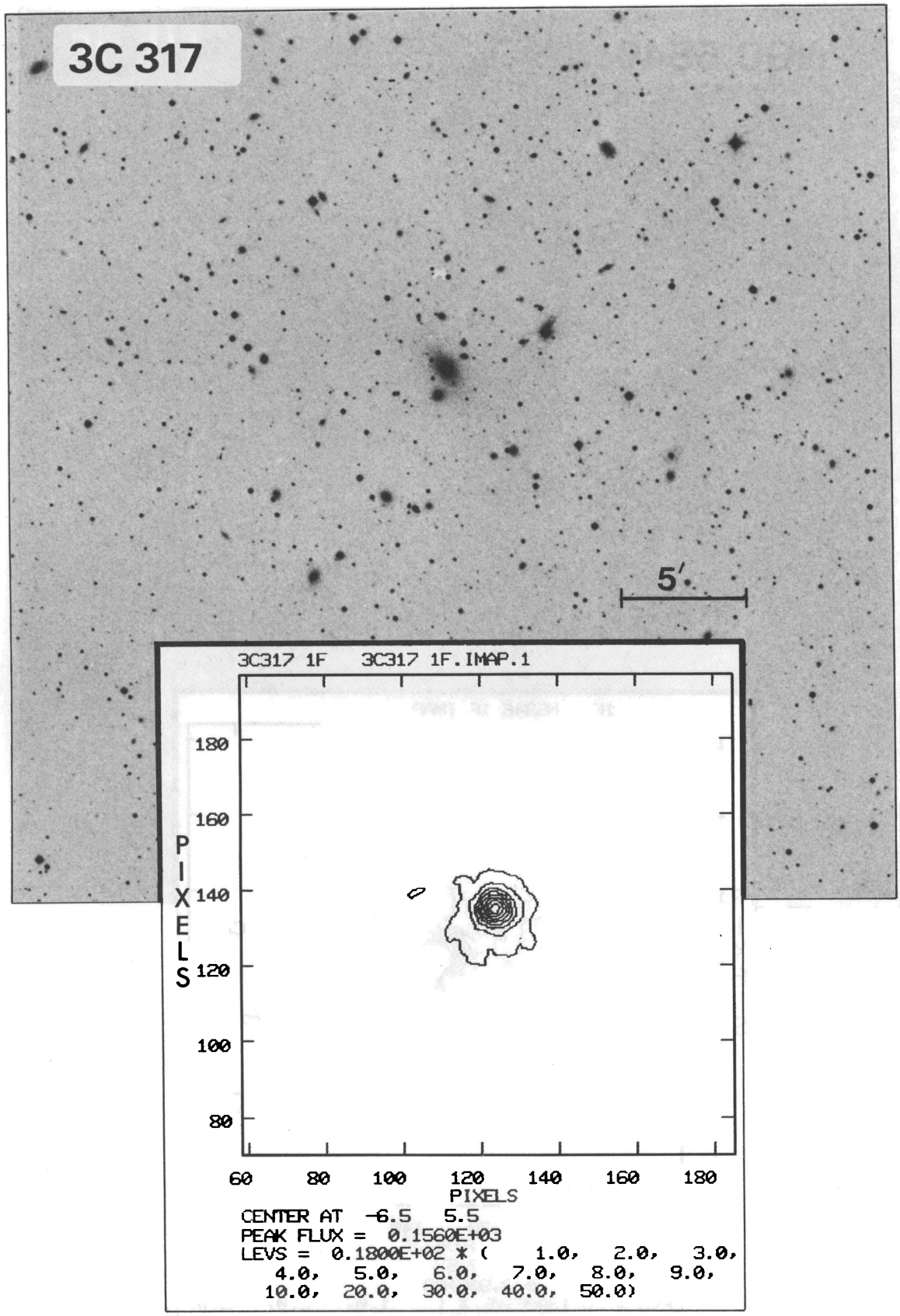


FIG. 7.—Same as Fig. 1 for NGC 3C 317. 10″ = 10 kpc.

TABLE 3

VELOCITIES OF THE IONIZED GAS

| | $r$ (arcsec) | $V_0$ (km s$^{-1}$) |
|---|---|---|
| NGC 2974: P.A. 45, N II, High | | |
| NE | 5.9–10.3 | 2155 |
| | 3.7 | 2050 |
| | 1.5 | 1995 |
| | 0.6 | 1825 |
| | 2.8 | 1685 |
| | 5.0 | 1645 |
| SW | 7.2–12 | 1650 |
| NGC 2974: P.A. 135, O II, Low | | |
| SE | 6.5–10.9 | 1875 |
| | 4.4 | 1845 |
| | 2.2 | 1880 |
| | 0 | 1870 |
| | 2.2 | 1805 |
| NW | 4.4 | 1885 |
| NGC 3962: P.A. 6, O II, High | | |
| S | 5.0 | 1890 |
| | 3.3 | 1795 |
| | 1.6 | 1795 |
| | 0 | 1795 |
| N | 1.6 | 1785 |
| NGC 3962: P.A. 6, Hα + N II, High | | |
| S | 2.4–4.1 | 1885 |
| | 0.8 | 1782 |
| N | 0.8–4.1 | 1805 |
| NGC 3962: P.A. 66, O II, High | | |
| NE | 4.1 | 1925 |
| | 2.5 | 1800 |
| | 0.8 | 1770 |
| | 0.8 | 1740 |
| | 2.5 | 1725 |
| SW | 4.1 | 1715 |
| NGC 3962: P.A. 66, Hα + N II, High | | |
| NE | 0.8 | 1845 |
| SW | 0.8 | 1735 |
| NGC 3962: P.A. 96, O II, High | | |
| E | 1.6 | 1905 |
| | 0 | 1800 |
| | 1.6 | 1750 |
| W | 3.3–5.0 | 1740 |
| NGC 3692: P.A. 96, Hα + N II, High | | |
| E | 2.4–5.7 | 1875 |
| | 0.8 | 1860 |
| | 0.8 | 1755 |
| W | 2.4–5.7 | 1690 |
| NGC 3692: P.A. 170, O I, Low | | |
| S | 4.4–8.7 | 1780 |
| | 2.2 | 1735 |
| | 0 | 1800 |
| | 2.2 | 1770 |
| N | 4.4–8.7 | 1720 |
| 3C 317: P.A. 0, O II, Low | | |
| | 2.2 | 10315 |
| | 0 | 10220 |
| | 2.2 | 10150 |

| | $r$ (arcsec) | $V_0$ (km s$^{-1}$) |
|---|---|---|
| NGC 4278: P.A. 25, Hα + N II, High | | |
| NE | 1.6 | 740 |
| | 0 | 640 |
| SW | 1.7 | 530 |
| NGC 4278: P.A. 25, O II, High | | |
| NE | 8.7 | 890 |
| | 7.1 | 740 |
| | 5.4 | 780 |
| | 3.8 | 760 |
| | 2.1 | 790 |
| | 0.5 | 680 |
| | 1.1 | 540 |
| | 2.8 | 480 |
| | 4.5 | 455 |
| SW | 6.1 | 485 |
| NGC 4278: P.A. 63, Hα + N II, High | | |
| NE | 8–11.6 | 835 |
| | 5–6.6 | 795 |
| | 3.3 | 780 |
| | 1.6 | 780 |
| | 0 | 650 |
| | 1.6 | 495 |
| NGC 4728: P.A. 63, O II, High | | |
| NE | 14–17.3 | 890 |
| | 9.1–12.4 | 810 |
| | 7.4 | 805 |
| | 5.8 | 795 |
| | 4.1 | 750 |
| | 2.5 | 695 |
| | 0.8 | 700 |
| | 0.8 | 625 |
| | 2.5 | 535 |
| | 4.1 | 455 |
| | 5.8 | 455 |
| | 7.4 | 455 |
| | 9–12.3 | 450 |
| SW | 14–17.3 | 410 |
| NGC 4728: P.A. 108, Hα + N II, High | | |
| SE | 2.5 | 675 |
| | 0.8 | 660 |
| | 0.8 | 630 |
| NW | 2.5 | 580 |
| NGC 4728: P.A. 108, O II, High | | |
| SE | 14.8–18.1 | 675 |
| | 9.9–13.2 | 645 |
| | 8.2–9.9 | 605 |
| | 6.6 | 660 |
| | 5.0 | 680 |
| | 3.3 | 670 |
| | 1.6 | 680 |
| | 0 | 655 |
| | 1.6 | 585 |
| | 3.3 | 580 |
| | 4.9–6.6 | 565 |
| | 8.2–9.9 | 590 |
| NW | 11.5–16.5 | 480 |
| NGC 4728: P.A. 153, Hα + N II, High | | |
| SE | 3.0 | 550 |
| | 1.3 | 590 |
| | 0.3 | 665 |
| NW | 2.0 | 690 |

TABLE 3—*Continued*

| | $r$ (arcsec) | $V_0$ (km s$^{-1}$) |
|---|---|---|
| NGC 4728: P.A. 153, O II, High | | |
| SE | 3.3 | 530 |
| | 1.6 | 625 |
| | 0 | 655 |
| | 1.6 | 715 |
| | 3.3 | 705 |
| NW | 5.0 | 710 |
| NGC 4728: P.A. 180, O II, High | | |
| S | 2.3 | 560 |
| | 0.7 | 590 |
| N | 1.0 | 700 |
| NGC 4728: P.A. 180, O II, Low | | |
| S | 5.8 | 600 |
| | 4.1 | 540 |
| | 2.5 | 610 |
| | 0.8 | 635 |
| | 0.8 | 650 |
| | 2.5 | 700 |
| | 4.1 | 730 |
| | (5.8) | (815) |
| N | 10.7 | 800 |
| NGC 4728: P.A. 63, O II, Low | | |
| NE | 14.6 | 780 |
| | 12.4 | 785 |
| | 10.2 | 825 |
| | 8.1 | 825 |
| | 5.9 | 790 |
| | 3.7 | 780 |
| | 1.5 | 720 |
| | 0.6 | 580 |
| | 2.8 | 460 |
| | 5.0 | 400 |
| | 7.2 | 460 |
| | 9.4 | 490 |
| SW | 11.6 | 530 |
| NGC 4636: P.A. 0, O II, Low | | |
| | 4.4–8.7 | 865 |
| | 2.2 | 915 |
| | 0 | 930 |
| | 2.2 | 950 |
| NGC 5077: P.A. 66, O II, High | | |
| NE | 6.2 | 2960 |
| | 4.5 | 2920 |
| | 2.9 | 2895 |
| | 1.2 | 2865 |
| | 0.4 | 2800 |
| | 2.1 | 2700 |
| | 3.7 | 2670 |
| | 5.4 | 2635 |
| | 7.0 | 2570 |
| SW | 8.7–17.0 | 2630 |
| NGC 5077: P.A. 66, Hα + N II, High | | |
| NE | 0.4 | 2960 |
| SW | 1.2 | 2860 |
| NGC 5077: P.A. 66, O II, Low | | |
| NE | 3.3 | 2820 |
| | 1.6 | 2865 |
| | 0 | 2795 |
| | 1.6 | 2730 |
| | 3.3 | 2630 |
| | 4.9 | 2630 |
| | 6.6–8.2 | 2580 |
| SW | 9.9–11.5 | 2635 |
| NGC 5077: P.A. 90, O II, High, 1979 | | |
| W | 10.7–15.7 | 2590 |
| | 9.1 | 2525 |
| | 7.4 | 2595 |
| | 5.8 | 2610 |
| | 2.5 | 2685 |
| | 0.8 | 2810 |
| | 0.8 | 2850 |
| | 2.5 | 2935 |
| | 4.1 | 2970 |
| | 5.8 | 2990 |
| | 7.4 | 3025 |
| | 9.1 | 3045 |
| E | 10.7 | 3055 |
| NGC 5077: P.A. 90, O II, High, 1980 | | |
| E | 8.7–10.9 | 2935 |
| | 6.5 | 3010 |
| | 4.4 | 2935 |
| | 2.2 | 2905 |
| | 0 | 2865 |
| | 2.2 | 2805 |
| | 4.4 | 3785 |
| | 6.5 | 2625 |
| | 8.7 | 2625 |
| | 10.9 | 2550 |
| W | 15.3–17.4 | 2550 |
| NGC 5077: P.A. 118, Hα + N II, High | | |
| SE | 1.2 | 2850 |
| NW | 0.5 | 2795 |
| NGC 5077: P.A. 118, O II, High | | |
| | 4.4–9.4 | 2965 |
| | 2.8 | 2915 |
| | 1.1 | 2840 |
| | 0.5 | 2785 |
| | 2.1 | 2770 |
| NW | 3.8 | 2710 |
| NGC 5846: P.A. 0, O II, High | | |
| S | 3.3 | 1665 |
| | 1.1 | 1695 |
| | 1.1 | 1640 |
| N | 3.3 | 1655 |
| NGC 5876: P.A. 90, O II, High | | |
| E | 0.8 | 1755 |
| | 3.0 | 1660 |
| W | 4.0–8.2 | 1580 |

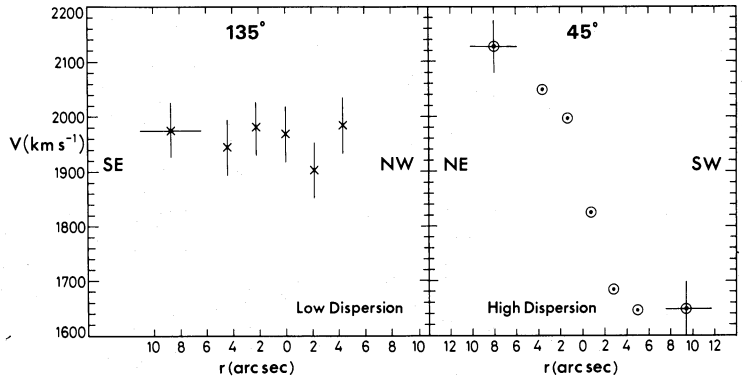


FIG. 8.—Velocities of the gas along the major (P.A. 45°) and minor (P.A. 135°) axes in NGC 2974. Low-dispersion data come from [O II] λ3727; high-dispersion data come from [N II] λ6584.

0.5 which indicates an inclination on the line of sight of 30° if these contours are circular in space.

The radio continuum in NGC 4278 and NGC 5077 has recently been mapped with the Very Large Array by Dr. Joan Wrobel who has kindly communicated some of her results prior to publication. Comparison of the 6 cm maps obtained by J. Wrobel with the distribution of the ionized gas does not reveal a correlation between the radio emission and the optical line emission. This is in contrast with the situation in some Seyfert galaxies (e.g., NGC 4151 [Wilson and Ulvestad 1982]) or radio galaxies (e.g., Coma A and 3C 305 [Miley *et al.* 1981; Heckman *et al.* 1982]) where there is a definite correlation between the distribution of the radio emission and the location of the ionized gas suggesting that the gas is compressed and excited by the particles producing the radio source. Mapping of the radio emission in NGC 4278 and NGC 5077 at a deeper level might, of course, reveal such a correlation.

## IV. THE VELOCITY FIELD OF THE GAS

### *a) General Results*

The velocity curves measured from the IPCS data approximately cover the same regions where the ionized gas was detected with the Video Camera. The velocities of the ionized gas in the galaxies for which we have the most data are listed in Table 3 and plotted as a function of the distance from center in Figures 8–12. The internal error estimated from repeated measurements is $\sigma \approx 30$ km s$^{-1}$ and 50 km s$^{-1}$ for the high- and low-resolution spectra, respectively, and $r < 8''$. For $r > 8''$, the error is larger and not well known because of the paucity of repeated measurements; our estimate for the high-dispersion data and $r > 8''$ is $\sim 50$ km s$^{-1}$.

There is some uncertainty associated with the use of the unresolved [O II] doublet for velocity measurements, because the intensity ratio of the components varies with the electron density $N_e$. In the very central region the ratio $I$([S II] λ6717)/$I$([S II] λ6731) is approximately 1, indicating $N_e \approx 1000$ cm$^{-3}$ for $T_e \approx 10^4$ K (Osterbrock 1974). The effective wavelength of the [O II] doublet for this density is 3727.24 Å. At the low-density limit the effective wavelength of the [O II] doublet is 3727.68. The maximum shift in wavelength caused by the maximum change of $N_e$ consistent with the ratios observed is therefore 0.44 Å or 35 km s$^{-1}$. The effect of the increase in effective wavelength with decreasing $N_e$ and thus with increasing $r$ appears to be present in our most accurate measurements, those made in P.A. 243° and P.A. 270° in NGC 4278 and NGC

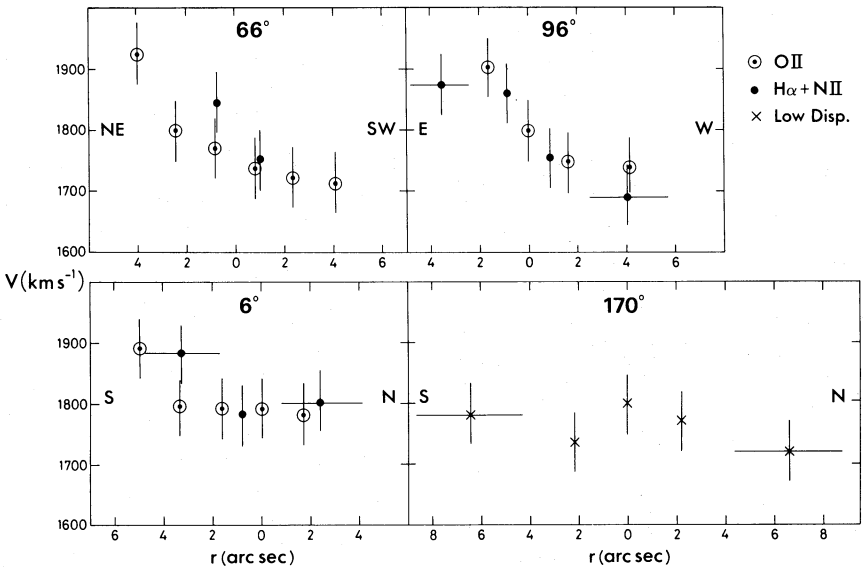


FIG. 9.—Velocities in NGC 3962

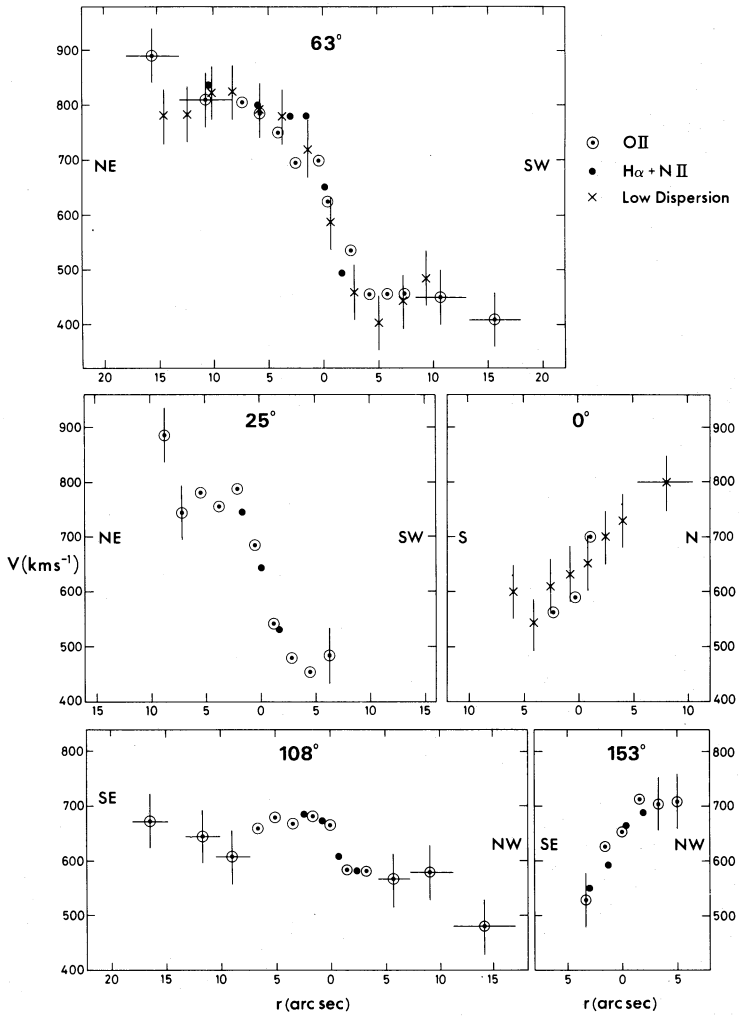


FIG. 10.—Velocities in NGC 4278

5077. In both instances the half-sum of the velocity measured at two points 5″ on either side of the nucleus is larger by $\sim 30 \pm 10$ km s$^{-1}$ than the velocity at center. This is consistent with the actual velocity curves being symmetrical with respect to the nucleus. The velocities in Figures 8–12 and Table 4 were obtained using $\lambda_{O\,II} = 3727.68$ Å.

A general feature apparent on all spectra of the galaxies which we observed is that the emission-line width is largest in the 1 or 2 central pixels and decreases rapidly outside the nucleus (see below Fig. 15). In NGC 4278, our best studied case, the FWHM of the lines at the center is $450 \pm 80$ km s$^{-1}$, corresponding to $\sigma = 191 \pm 25$ km s$^{-1}$, which within the errors is similar to the value of 220 km s$^{-1}$ measured by Schechter and Gunn (1979) for the velocity dispersion of the stars at the center. Away from the center the velocity dispersion of the gas drops to less that 150 km s$^{-1}$. In the central increments of the spectra of NGC 4278 and NGC 5077, there seems to be some structure at the limit of the wavelength and angular resolution. Observations under excellent seeing conditions and higher wavelength resolution might reveal the presence of several clouds, possibly in ordered motions with respect to the center, instead of one cloud with a large velocity dispersion.

The pattern of the velocity curves shown in Figures 8–12 suggests and is consistent with a velocity field which is primarily caused by rotation around the nucleus. With the assumption that the gas in each galaxy is in a rotating disk, we have determined the position angle of the kinematic major axes by comparing the values of the velocity gradient at center for the various slit positions with the cosine curve expected for pure rotation. The values are given in Table 1, column (7).

### *b) The Case of NGC 4278*

Schechter and Gunn (1979) find that the dynamical major axis of the stellar population in NGC 4278 is between 0° and 20°. Raimond *et al.* (1981) interpret the velocity field in H I as being caused by a rotating oval ring with its kinematic major axis in P.A. 65° ± 5° and its kinematic minor axis in P.A. 140° ± 3°. The accuracy of the measurements of the emission lines presented here does not permit one to detect a discrepancy from perpendicularity between the kinematic major and minor axes of the ionized gas similar to the one found in H I. Our best estimate of the position angle of the kinematic major axis of the ionized gas is 40° ± 12°. The position angle of the kinematic minor axis of the ionized gas is 130° ± 12° which is

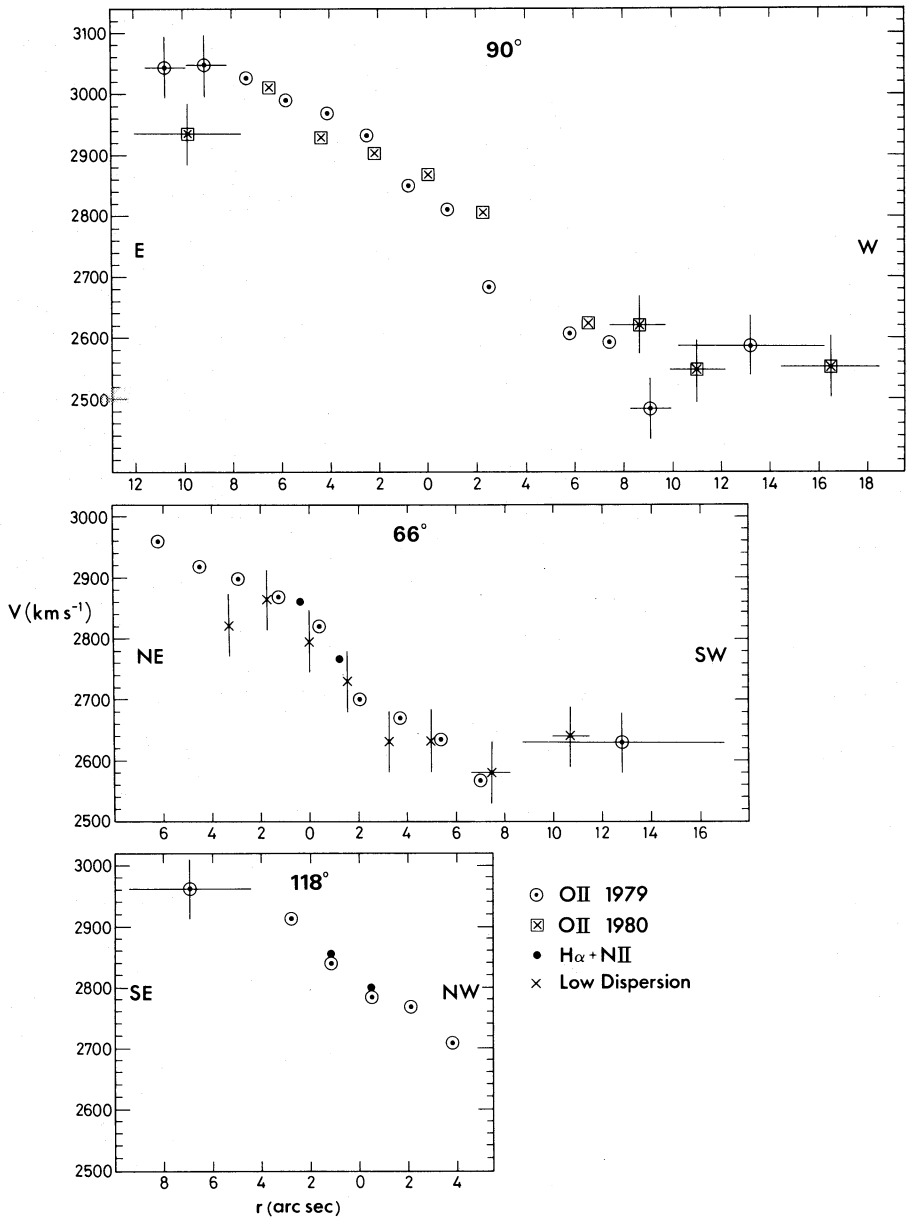


FIG. 11.—Velocities in NGC 5077

barely compatible with the value of 140° ± 3° for the oval ring of H I.

In summary, the neutral gas ring and the ionized gas disk appear to differ by their apparent ellipticity and by the position angles of their kinematic major axes.

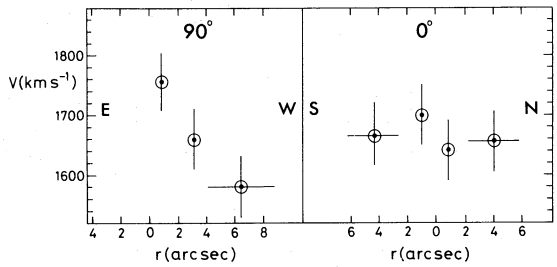


FIG. 12.—Velocities in NGC 5846

One possible interpretation is that that the neutral and the ionized gas follow normal prograde closed orbits in the equatorial plane of the potential of a triaxial galaxy. The orbits, in this case, are elliptical with their major axes perpendicular to the long axis of the potential and have different ellipticities (Contopoulos and Papayannopoulos 1980). These properties of the normal orbits can explain the difference in the apparent ellipticities and the difference in the direction of the kinematic major axis of the neutral gas and of the ionized gas.

On the other hand the gas cloud may not yet have reached stable orbits. The progression of the direction of the rotation axes for the stars, the ionized gas and the neutral gas, together with the different inclination along the line of sight for the H I ring and the gas disk—if the ring and the disk can be assumed to be circular in first approximation—suggests that the gas is in differential precession with the ionized gas being closer to settling in the equatorial plane than is the neutral gas which is located farther out.

Finally it is interesting to compare the velocities of the gas observed in NGC 4278 with the rotation velocities in a spherical galaxy. Figure 13 shows the rotation curve in a spherical galaxy obeying the $r^{1/4}$ law in projection, with a total mass $M_T = 1.5 \times 10^{11}\ M_\odot$ and an effective radius $r_e = 4$ kpc (Young 1976). The data points at 5″ and 10″ are the average of the NE and SW velocities in PA 63°; $v_{obs} = 163$ km s$^{-1}$ and 187 km s$^{-1}$, respectively. The point at 1.5 comes from the observed H I velocity, $v = 175$ km s$^{-1}$ (Raimond *et al.* 1981). All three velocities are corrected for the same assumed inclination of the line-of-sight of 45°. The thin line in Figure 13 is the rotation curve for a galaxy with $r_e = 8$ kpc and $M_T = 8 \times 10^{11}\ M_\odot$ (or $M_B = -21.0$ for $M/L = 20$).

The possibly fortuitous agreement between the three observed points and the calculated rotation curve points to the necessity of obtaining accurate measurements and of observing many galaxies in order to identify the effects of nonsphericity and to neutralize the projection effects. In this respect it is interesting to note that a disk of gas has a probability of 0.5 of having an inclination on the line of sight of $i < 30°$. If the velocities can in first approximation be assumed to be circular the values $i < 30°$ give $v_{obs} = v_{cir} \cos i \approx v_{obs}$. Large velocities of the gas (up to ~450 km s$^{-1}$) are therefore not unexpected when one observes a fair number of massive ellipticals ($M_T \approx 8 \times 10^{11}\ M_\odot$). The observed velocity of the stars is of course smaller since it is the sum of the figure rotation and of the streaming motion (Miller and Smith 1979; Schwarzschild 1982).

### c) *The Other Galaxies*

*NGC 2974.*—The ionized gas has a well-ordered velocity field consistent with a disk in rotation around the minor axis of the outer stellar isophotes. The isophotes of the ionized gas on the other hand are more nearly circular than disklike.

*NGC 3962.*—The velocity curves are consistent with a disk in rotation around the apparent major axis of the galaxy. The distribution of the ionized gas is elliptical, but with a major axis skewed with respect to the rotation and stellar major axes.

*NGC 3773.*—This is a nearby dwarf object. The line intensity ratio Hα/[N II] λ6584 is equal to ~10. The emission lines are intense and yield velocity measurements of high accuracy. No gradient larger than 30 km s$^{-1}$ for 10″ is detected in P.A. 0° and 90°. The emission lines have the instrumental profile. The width of the H I line is 118 km s$^{-1}$ (Knapp, Kerr, and Henderson 1979).

*NGC 4636.*—We find a gradient of velocity of ~100 km s$^{-1}$ for 9″ in P.A. 0°. The major axis of the stellar isophotes is 152°, and Davies (1981) reports a maximum velocity of the stars of 60–80 km s$^{-1}$ along this axis. The galaxy appears fairly isolated with a prominent population of globular clusters. Our imaging data show weak or no line emission from the nucleus proper, and our map in Figure 4 exhibits a hole in the emission at the position of the nucleus.

*NGC 5077.*—We have no measurement in P.A. ≈ 0°, but the similarity of the velocity gradients in P.A. 66°, 90°, and 118° suggests that the direction of the rotation axis of the ionized gas is close to 0° which is the direction of the major axis of the stellar component.

*NGC 5846.*—We have only two position angles. The velocity data suggest that the dynamical major axis is close to P.A. 90°. The major axis of the outer isophotes of the stellar population is 64° (King 1978), but the ellipticity is very small. No velocity gradient of the stellar component has been found in P.A. 78° (Peterson 1978).

*3C 317.*—Measurement along the major axis of the stellar population gives a gradient of the gas velocity of 220 km s$^{-1}$ per 6″.

## V. IONIZATION MECHANISMS

Spectrophotometric observations of NGC 2974, NGC 3962, and NGC 5077, and for comparison NGC 1052 were made with the ESO Image Dissector Scanner (IDS) to avoid possible

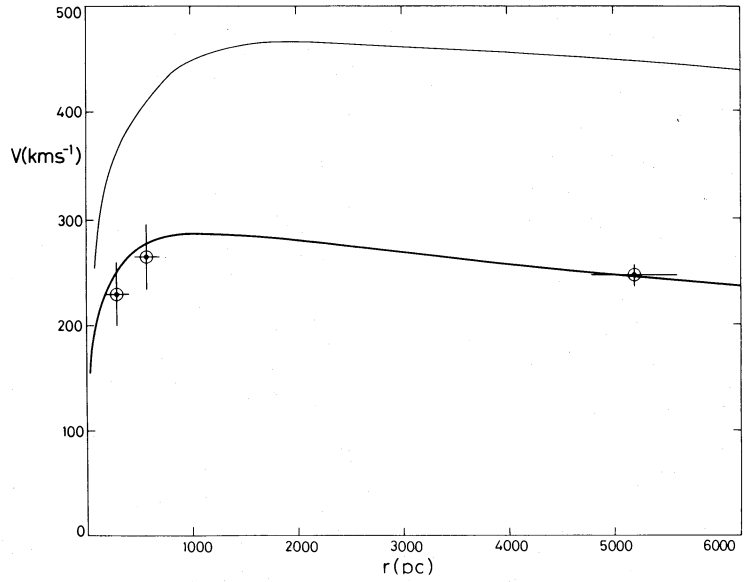


FIG. 13.—Thick line represents the velocity of rotation in a spherical galaxy obeying the $r^{1/4}$ law, with a total mass $M_T = 1.5 \times 10^{11}\ M_\odot$ and an effective radius $r_e = 4$ kpc. Data points at 5″ and 10″ (0.6 and 0.9 kpc) are the measurements in P.A. 63° in NGC 4278 (this paper, Fig. 10). The point at 5.2 kpc is from Raimond *et al.* (1981). All observed velocities have been corrected for an assumed inclination on the line of sight of 45°. Thin curve is same as thick curve for $M_T = 8 \times 10^{11}\ M_\odot$ and $r_e = 8$ kpc.

TABLE 4

RELATIVE LINE INTENSITIES

| Line | NGC 2911 | NGC 2974 | NGC 3962 | NGC 5077 | NGC 5077 "A" | M87 Filament |
|---|---|---|---|---|---|---|
| [O II] λ3727 | ... | 1.36: | 1.63: | 1.67: | ... | 1.45 |
| Hβ λ4861 | ... | 0.21: | ... | ... | ... | ... |
| [O III] λ5007 | ... | 0.31 | 0.35 | 0.42 | ... | 0.57 |
| [O I] λ6300 | 0.11 | <0.23 | 0.18 | 0.50 | 0.25 | 0.32 |
| [N II] λ6548 | 0.68 | 0.86 | 1.0 | 0.53 | 0.25 | ... |
| Hα λ6563 | 1.00 | 1.0 | 1.0 | 1.00 | 1.00 | 1.00 |
| [N II] λ6583 | 1.61 | 2.53 | 2.20 | 1.14 | 0.74 | 2.52 |
| [S II] λ6716 | 0.89 | 0.58 | 1.18 | 0.84 | 0.84 | 0.86 |
| [S II] λ6731 | 0.09 | 0.60 | 1.27 | 0.63 | 0.88 | 0.74 |

saturation effects with the IPCS. The northern galaxy NGC 4278 was observed at KPNO with the IDS attached to the 2.1 m telescope. The line intensities scaled to $I(\mathrm{H}\alpha)$ are given in Table 4 except for the line intensities in NGC 4278 which are scaled to $I(\mathrm{H}\beta)$ and are given in Table 5. The intensities of Hα and Hβ in emission have been corrected for the effect of the absorption lines of the stellar population by subtracting the spectrum of a typical elliptical galaxy. No correction for reddening has been attempted because of the weakness of the Hβ emission line in most of the galaxies observed. Some of the spectra are shown in Figures 14 and 16.

Spectrophotometric observations in the range 6200–7000 Å were also made at one point in the extended emission region of NGC 1052, NGC 4278, and NGC 5077 (Fig. 15). In each case it is found that the lines are narrower in the nebulosity than in the nucleus, consistent with the IPCS data, and that the line intensity ratios are, within the rather large measurement errors, the same in the nebulosity and in the nucleus.

It is easy to show that without a continuous supply of energy the gas would recombine in less than $10^6$ yr. Let us take the example of the nucleus of NGC 4278. The Hβ intensity from a region 2 arcsec$^2$ at the center is $I(\mathrm{H}\beta) = 3 \times 10^{-14}$ ergs cm$^{-2}$ s$^{-1}$, corresponding to $L(\mathrm{H}\beta) \approx 10^{39}$ ergs s$^{-1}$. The line intensity ratio $I$(S II λ6716)/$I$(S II λ6731) is ~1 indicating $N_e \approx 500$ cm$^{-3}$. The mass of the ionized gas is thus $10^5\ M_\odot$. The kinetic energy of the ionized gas is $\sim 4 \times 10^{52}$ ergs, and therefore the energy available transformed into Hβ photons would be exhausted in $10^4$ yr (assuming that only 1% of the kinetic energy is transformed into Hβ photons). Even if the density were ~10 cm$^{-3}$, which is the smallest value possible since it corresponds to a filling factor of ~1, the lifetime of the ionized region would be only $\sim 10^6$ yr. Such a short lifetime is not compatible with the fraction of ellipticals with emission lines in their spectrum and therefore implies that there is a continuous source of energy.

TABLE 5

RELATIVE LINE INTENSITIES IN NGC 4278

| Line | Intensity |
|---|---|
| [O II] λ3727 | 6.2 |
| [Ne III] λ3869 | 0.3 |
| H I λ3889 | 0.3 |
| [Ne III] λ3968 + H I λ3970 | 0.3 |
| [S II] λλ4069, 4076 | 0.3 |
| H I λ4101 | 0.4 |
| Hγ | 0.45 |
| [O III] λ4363 | <0.20 |
| Hβ | 1.0 |
| [O III] λ4959 | 0.5 |
| [O III] λ5007 | 1.4 |
| [O I] λ6300 | 0.6 |
| [N II] λ6548 | 1.8 |
| Hα | 3.3 |
| [N II] λ6583 | 4.1 |
| [S II] λ6716 | 2.4 |
| [S II] λ6731 | 2.1 |

In this section we consider energy sources which are related to the stellar population (such as mass loss from evolved stars, supernovae, and UV continuum of stellar origin) and energy sources which are independent of the stellar population, namely the accretion of gas from an external system and the effect of a nonthermal UV source in the nucleus. At this point, we concern ourselves only with the *total* energy provided by these energy sources rather than by the detailed processes by which the energy is given to the gas.

The estimate of the energy necessary to keep the gas ionized is based on the following figures for the efficiency with which Hβ photons are produced: (*i*) In the case of photoionization it is assumed that case B recombination is valid and that one Hβ photon corresponds to 9.3 ionizing photons. (*ii*) In the case of ionization by shocks we take $\epsilon = 0.01$ for the efficiency with which kinetic energy is transformed into radiative energy in the form of Hβ photons. This figure is uncertain because it depends on the shock velocity $V$ and on the density $N$ of the preshocked gas. In the model H of Shull and McKee (1979) where $V = 100$ km s$^{-1}$ and $N = 10$ cm$^{-3}$, the value of $\epsilon$ is $\sim 0.4 \times 10^{-2}$.

### *a) Energy Provided by the Stellar Population: Ultraviolet Photons, Mass Loss, and Supernovae*

It is assumed that the spectrum of all elliptical galaxies is similar to that of NGC 4472 in which the ratio $L_\lambda$(1000

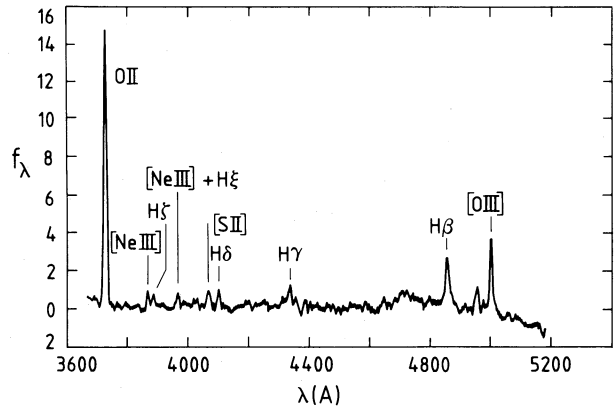


FIG. 14.—The spectrum of the nucleus of NGC 4278 after subtraction of the spectrum from the stellar population.

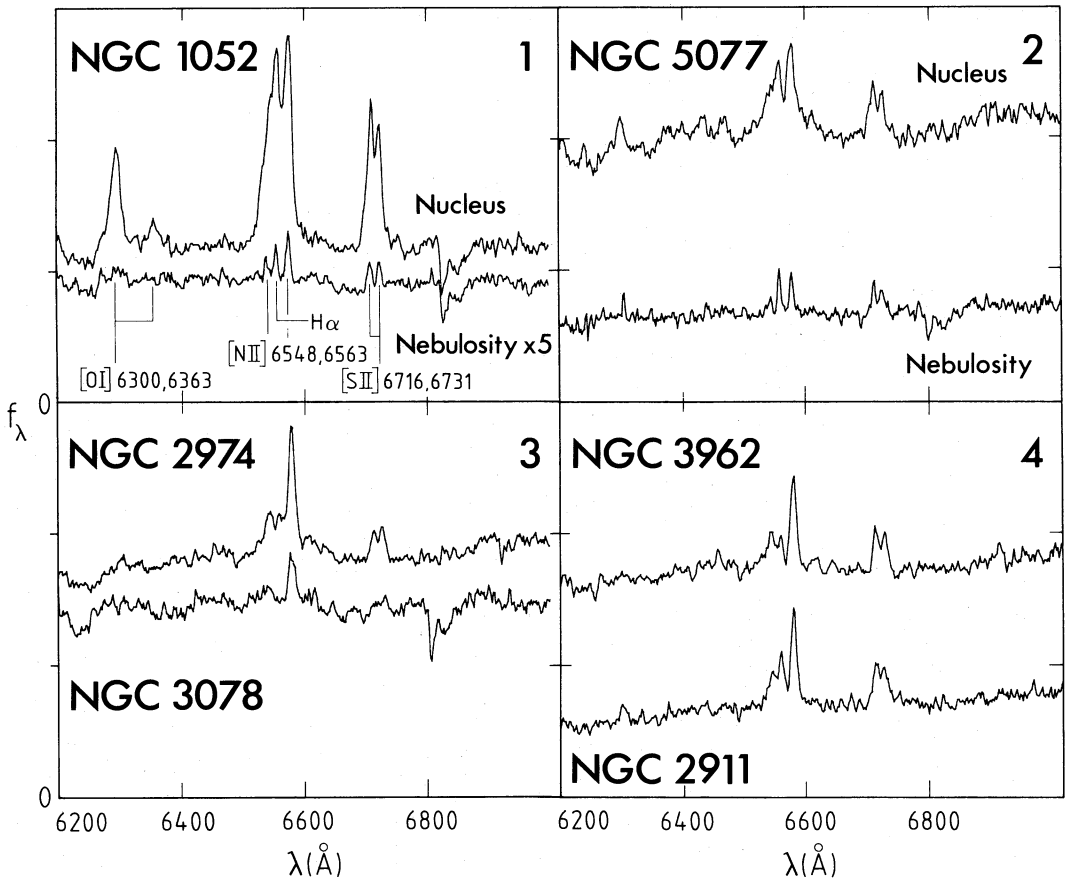


FIG. 15.—(*top*) 1 and 2: Spectrum near Hα of the nucleus and of the nebulosity in NGC 1052 and NGC 5077. Note the narrow lines in the nebulosity. (*bottom*) 3 and 4: Spectrum near Hα of the nucleus of NGC 2974, NGC 3078, NGC 3962, and NGC 2911.

Å)/$L_\lambda$(4860 Å) is equal to 0.1 (Oke, Bertola, and Capaccioli 1980). It is further assumed that the ultraviolet radiation is emitted by 30,000 K stars (probably horizontal-branch stars). Ionization by stars at very high temperatures, $\sim 10^5$ K, would normally give $I$(O II λ3727)/$I$(O II λ5007) < 1, contrary to what is observed. There is the possibility that most of [O II] λ3727 would come from not very ionized clouds temporarily shielded from the ionization sources, but this is a rather contrived model. The unambiguous diagnostic for the shape of the ionizing continuum below 912 Å is to measure or obtain significant upper limits to the intensity of the lines of highly ionized species. For example, the detection of [Ne V] λ3426 with a ratio $I$(Ne V λ3426)/$I$(O III λ5007) > 0.1 would be the signature of the ionization by very hot stars or by a nonthermal source. The observed $I$(O II λ3727)/$I$(O III λ5007) ratio is consistent with ionization by stars at ~30,000 K, and it is this value which is used in the following discussion.

A portion of an elliptical galaxy having $10^9$ $L_\odot$ emits a flux

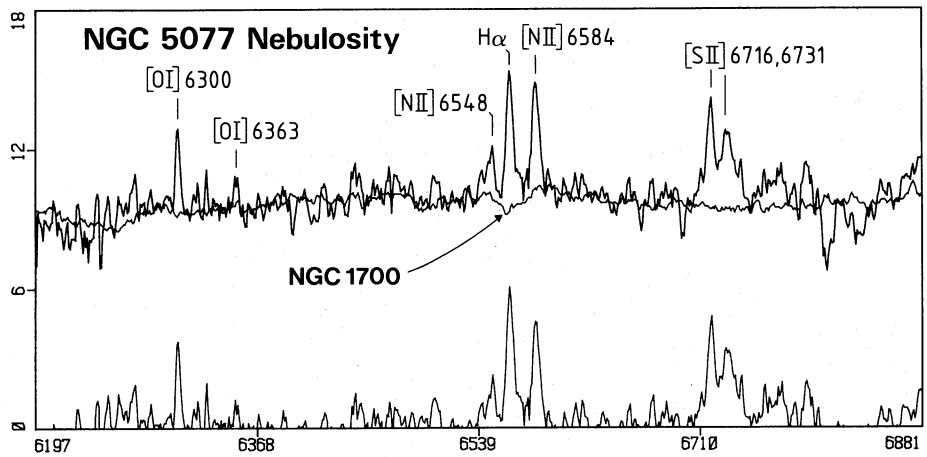


FIG. 16.—Example of the subtraction of the stellar population. In this case a scaled spectrum of the elliptical NGC 1700 is subtracted from the spectrum of NGC 5077 outside the nucleus.

$L_\lambda = 9.5 \times 10^{38}$ ergs s$^{-1}$ Å$^{-1}$ at 4860 Å or $9.5 \times 10^{37}$ ergs s$^{-1}$ Å$^{-1}$ at 1000 Å. The collection of 30,000 K stars which can emit this flux at 1000 Å emits $1.2 \times 10^{50}$ ionizing photons (Hummer and Mihalas 1970; Kurucz 1979). This is sufficient for keeping ionized a gas cloud intercepting all the ionizing photons and emitting $L(\mathrm{H}\beta) = 5 \times 10^{37}$ ergs s$^{-1}$. The ratio $L(\mathrm{H}\beta)/L_\lambda(4860)$ is the equivalent width of H$\beta$ of the $10^9$ $L_\odot$ region considered here and is equal to $\sim$0.05 Å. If this region is located inside a galaxy, the observed equivalent width of H$\beta$ will be smaller because of the contribution of the stars which are along the line of sight and outside the region. The conclusion is that the UV photons from the normal stellar population cannot keep ionized a gas cloud with $\mathrm{EW}(\mathrm{H}\beta)_{\mathrm{obs}} > 0.1$ Å.

Regarding the energy provided locally by the stellar wind, we use the estimate of 0.015 $M_\odot$ per year per $10^9$ $L_\odot$ and a wind velocity of 150 km s$^{-1}$. This corresponds to an input of $10^{38}$ ergs s$^{-1}$, which can produce $L(\mathrm{H}\beta) = 10^{36}$ ergs s$^{-1}$ (using $\epsilon = 0.01$ for the efficiency with which kinetic energy is transformed into H$\beta$ photons). Thus the energy yielded to the interstellar medium by the stellar wind cannot keep ionized a gas cloud whose equivalent width is larger than $10^{-3}$ Å.

Finally, for the energy supplied through supernova explosions, we use the commonly quoted figure of $10^{51}$ ergs per explosion (Woltjer 1972) and the estimate by Tammann (1974) of $2.5 \times 10^{-4}$ supernovae per year per $10^9$ $L_\odot$. The energy input is $7.9 \times 10^{39}$ ergs s$^{-1}$ corresponding to $L(\mathrm{H}\beta) = 7.9 \times 10^{37}$ ergs s$^{-1}$ and to a maximum equivalent width of 0.1 Å.

The equivalent width of the H$\beta$ line produced by shock ionization by stellar mass loss and by supernovae explosions is $10^{-3}$ Å and $10^{-1}$ Å, respectively. It seems therefore that the energy input of the stellar population is insufficient to produce H$\beta$ lines which have an equivalent width larger than 0.1 Å, the supernovae explosions being the process which comes closer to keeping the gas ionized.

The equivalent width of N II $\lambda$6584 measured at the center of NGC 2974, NGC 3962, NGC 4278, and NGC 5077 is $\sim$5 Å, 4.5 Å, 10 Å, and 3.5 Å, respectively. Taking $\mathrm{EW}(\mathrm{N\ II}\ \lambda6584)/\mathrm{EW}(\mathrm{H}\alpha) = 2$ and $I(\mathrm{H}\alpha)/I(\mathrm{H}\beta) = 2.9$, one obtains $\mathrm{EW}(\mathrm{H}\beta) \approx 1.6$ Å for NGC 4278 and $\mathrm{EW}(\mathrm{H}\beta) \approx 0.8$ Å for the three other galaxies. Since the distribution of the gas is more peaked than that of the stars, the equivalent width of a line increases toward the center. The central values given here are therefore only *indicative* as they depend on the seeing and on the positioning of the nucleus with respect to the detector increments. In spite of these uncertainties it appears that the emission lines observed in the center of these galaxies are too intense to be excited by processes related to the stellar population.

### b) *Other Sources of Energy*

One source of energy which is available in all elliptical galaxies is the kinetic energy of the gas shed by red giant stars as it approaches the central region of the galaxy. The energy input is calculated first in the case of NGC 4278. Most of the stars in an elliptical are within the radius where the velocity of escape from the galaxy is larger than the velocity of a red giant stellar wind, $\sim$150 km s$^{-1}$. Therefore nearly all the gas remains in the galaxy unless swept away by a supernova driven wind or by an intracluster medium. In NGC 4278 and the other galaxies considered here, gas is present in the center and therefore the sweeping mechanism is not at work presently.

The maximum energy that a mass of gas $\Delta m(r)$ produced at a radius $r$ can provide when it reaches the central region of the galaxy is $\Delta E = \Delta m(r) v_{\mathrm{ff}}{}^2(r)/2$, where $v_{\mathrm{ff}}$ is the free fall velocity of the gas starting at distance $r$ and arriving near the center. The integration of $\Delta E$ over the radius of the galaxy can be done easily for a spherical galaxy obeying the $r^{1/4}$ law (Young 1976). Using the same value for the mass loss rate as used above, and $M_T = 1.5 \times 10^{11}$ $M_\odot$ and $r_e = 4000$ pc which are the parameters approximately fitting NGC 4278, one finds $\Delta E = 10^{40}$ ergs s$^{-1}$, which corresponds to a maximum H$\beta$ luminosity of $10^{38}$ ergs s$^{-1}$. This figure is to be compared to the total observed luminosity $L_T(\mathrm{H}\beta)$ of the central disk of gas in NGC 4278. From the H$\alpha$ luminosity profiles obtained from the video camera frames in NGC 4278, it is estimated that the total luminosity of the gas cloud in H$\beta$, $L_T(\mathrm{H}\beta)$, is $\sim$4 times the luminosity in the central 2 arcsec$^2$ or $4 \times 10^{39}$ ergs s$^{-1}$. Therefore, in NGC 4278 the gas shed by the stars and falling on the disk of ionized gas at center does not provide enough energy to keep the gas ionized. However, NGC 4278 contains a large amount of neutral gas in a disk, making it a special case. This gas can be expected to interact with stellar mass loss material and slowly contract toward the center of the object. In doing so, it may see a changing, perhaps triaxial, potential, and therefore may not move in closed orbits. The individual clouds could then collide among themselves and so become ionized. We are unable to estimate the efficiency of such a process without a detailed knowledge of the galactic potential.

In galaxies which are more massive and have less intense emission lines than NGC 4278, the gas shed by stars may be sufficient. For example, this is the case for NGC 2974 which is 5 times more massive and where the total H$\beta$ line intensity is 3 times less than in NGC 4278.

Yet another possibility is that the gas in ellipticals is ionized by a weak nonthermal source. This possibility was first suggested by Péquignot (1981), then by Ferland and Netzer (1982), while ionization by shocks had been advocated earlier by Koski and Osterbrock (1976) on the basis of the strength of the [O III] $\lambda$4363 line which they had measured in NGC 1052. The new measurement of this line by Keel and Miller (1983) does not confirm the high values reported earlier, weakening the case for ionization by shocks. The situation is now open as to which mechanism, shocks or photoionization by a central nonthermal source, is relevant to this galaxy and other ellipticals. Further progress will come from models of shocks and of photoionization adapted to the nuclei of active galaxies, e.g., Péquignot (1983) (diluted radiation field, gradient of density, and overabundance of elements) and from the measurements of many more lines, in particular lines of highly ionized elements such as [Ne V] $\lambda$3426, since the 10 or so lines which are commonly measured (H$\alpha$, H$\beta$, [N II] $\lambda\lambda$6584, 6548, [S II] $\lambda\lambda$6731, 6717, etc. ...) do not constitute a good discriminant of the ionization mechanisms.

It is interesting to note that in the three galaxies NGC 1052, NGC 4278, and NGC 5077, which are in small groups, the intensity ratio [N II] $\lambda$6584/H$\alpha$ is less than 2 while it is larger than 2 in the other galaxies discussed here (see Fig. 10 and Table 5). One possible explanation for the low value of [N II]/H$\alpha$ is that the three galaxies are accreting gas having a low nitrogen abundance. Via the "classical black hole scenario" (Gunn 1979), this accretion can create the conditions for the formation of a central source producing the ionizing photons and the compact radio sources which are present in these three galaxies (van Breugel *et al.* 1981). All the distinctive properties of these three galaxies would then derive from the same pheno-

menon of gas accretion. This is only speculative and must be confirmed with more cases. In the case of M87 a cooling accretion flow of intracluster gas has been proposed as the source of the ionized gas near the center (Ford and Butcher 1979). In this galaxy the ratio [N II] $\lambda$6584/H$\alpha$ is larger than 2, which is consistent with the rather high metal content of the intracluster gas. The recent discovery of extended X-ray emission centered on NGC 5846 (Bierman and Kronberg 1983) indicates this galaxy, too, is probably undergoing significant amount of accretion, with the captured gas cooling towards the center.

That accretion of small amounts of matter (i.e., small compared to the total mass) onto normal elliptical galaxies is a rather common phenomenon has also been shown recently by Malin and Carter (1983) and Quinn (1983). These authors find that some 17% of normal isolated ellipticals show shell-like structures probably indicative of recent mergers with small, late-type systems. The gas from the smaller objects in these events can be expected to fall to the centers of the ellipticals, heating up in the process. Our data are not ideal for detection of the Malin-Carter shells, and we do not see evidence for their presence in any of our objects. The time scale for any incoming gas to migrate to the nucleus is likely to be somewhat longer than that for shell dissipation, so it is perhaps not surprising that we detect no shells.

## VI. CONCLUSIONS

We have found extended H II emission in the central regions of roughly half of a sample of normal elliptical galaxies with nuclear line emission. The gas appears to be more or less in rotational equilibrium, although the morphology of the detected regions is not disklike. The lack of a general correlation between the rotation axes of the gas and the rotation axes or the isophotes of the stellar populations can be explained either by the gas being in normal closed orbits in the equatorial plane of a triaxial galaxy or by having not yet reached stable orbits and being in differential precession. This could be the case if the gas is material shed by the stars through normal evolution or if it is material accreted from outside the main galaxy, a possibility which is supported by the recent discovery that shell-like isophotes resulting from mergers are fairly common in ellipticals.

Regarding the source of ionization of the gas we distinguish three situations with rather uncertain limits. For EW(H$\beta$) $\leq$ 0.1 Å, normal stellar processes such as ultraviolet stellar photons, stellar winds, and supernovae ejecta can supply the energy necessary to keep the gas ionized. For 0.1 $\lesssim$ EW(H$\beta$) $\lesssim$ 5 Å, the gas shed by stars and falling on the central disk of ionized gas seems to provide enough energy to ionize the gas. Beyond EW(H$\beta$) = 5 Å the source of energy is not directly related to a normal stellar population. It could be the accretion energy of gas captured from another galaxy or an intergalactic cloud, or a central nonthermal source. The distinction between these two sources of energy is not possible with the present material. Long-slit spectra with higher signal-to-noise ratios and larger wavelength coverage would allow one to measure or to obtain significant upper limits to the intensities of lines of highly ionized species such as [Ne V] $\lambda$3426 or He II $\lambda$4686 and thus to put some interesting constraints on the shape of the ionizing continuum. The same spectra would also give the extensive and precise data on the velocity field of the ionized gas which are necessary to set very stringent upper limits to the noncircular components of the velocity.

It is a pleasure to acknowledge stimulating discussions with D. Péquignot. We wish to thank J. Fordham and K. Shortridge for their cheerful assistance in using the IPCS at La Silla.

## REFERENCES

Biermann, P., and Kronberg, P. P. 1983, *Ap. J. (Letters)*, **268**, L69.
Boksenberg, A. 1978, in *ESO Conference Optical Telescopes of the Future*, ed. F. Pacini, W. Richter, and R. N. Wilson, p. 497.
Contopoulos, G., and Papayannopoulos, T. 1980, *Astr. Ap.*, **92**, 33.
Davies, R. L. 1981, *M.N.R.A.S.*, **194**, 879.
Faber, S. M., and Gallagher, J. S. 1976, *Ap. J.*, **204**, 365.
Ferland, G. J., and Netzer, H. 1983, *Ap. J.*, **264**, 105.
Ford, H. C., and Butcher, H. 1979, *Ap. J. Suppl.*, **41**, 147.
Gunn, J. E. 1979, in *Active Galactic Nuclei*, ed. C. Hazard and S. Mitton (Cambridge: Cambridge University Press), p. 213.
Heckman, T. M., Miley, G. K., Balick, B., van Breugel, W. J. M., and Butcher, H. R. 1982, *Ap. J.*, **262**, 259.
Heisler, J., Merritt, D., and Schwarzschild, M. 1982, *Ap. J.*, **258**, 490.
Humason, M. L., Mayall, N. U., and Sandage, A. R. 1956, *A.J.*, **61**, 97.
Hummer, D. G., and Mihalas, D. 1970, *M.N.R.A.S.*, **147**, 339.
Keel, W. C., and Miller, J. S. 1983, *Ap. J. (Letters)*, **266**, L89.
King, I. R. 1978, *Ap. J.*, **222**, 1.
Knapp, G. R., Kerr, F. J., and Henderson, A. P. 1979, *Ap. J.*, **234**, 448.
Koski, A. T., and Osterbrock, D. E. 1976, *Ap. J. (Letters)*, **203**, L49.
Kurucz, R. L. 1979, *Ap. J. Suppl.*, **40**, 1.
Malin, D. F., and Carter, D. 1983, *Ap. J.*, **274**, 534.
Mathews, W. G., and Baker, J. C. 1971, *Ap. J.*, **170**, 241.
Miley, G. K., Heckman, T. M., Butcher, H. R., and van Breugel, W. J. M. 1981, *Ap. J. (Letters)*, **247**, L5.
Miller, R. H., and Smith, B. F. 1979, *Ap. J.*, **227**, 785.
Oke, J. B., Bertola, F., and Capaccioli, M. 1981, *Ap. J.*, **243**, 453.
Péquignot, D. 1981, Ph.D. thesis, University of Paris.
———. 1983, *Astr. Ap.*, in press.
Peterson, C. J. 1978, *Ap. J.*, **222**, 84.
Quinn, P. J. 1983, in *IAU Symposium 100, Internal Kinematics and Dynamics of Galaxies*, ed. E. Athanassoula (Dordrecht: Reidel), p. 347.
Raimond, E., Faber, S. M., Gallagher, J. S., and Knapp, G. R. 1981, *Ap. J.*, **246**, 708.
Sancisi, R. 1981, in *The Structure and Evolution of Normal Galaxies*, ed. S. M. Fall and D. Lynden-Bell (Cambridge: Cambridge University Press), p. 149.
Sandage, A., Kristian, J., and Westphal, J. A. 1976, *Ap. J.*, **205**, 688.
Sandage, A. R., and Tammann, G. A. 1981, *A Revised Shapley-Ames Catalog of Bright Galaxies* (Washington, D.C.: Carnegie Institution of Washington).
Sanders, R. H. 1981, *Ap. J.*, **244**, 820.
Schechter, P. L., and Gunn, J. E. 1979, *Ap. J.*, **229**, 472.
Schwarzschild, M. 1982, *Ap. J.*, **263**, 599.
Shull, J. M., and McKee, C. F. 1979, *Ap. J.*, **227**, 131.
Tammann, G. A. 1974, in *Supernovae and Supernovae Remnants*, ed. C. B. Cosmovici, E. D'Anna, and A. Borghesi (Dordrecht: Reidel), p. 215.
Tohline, J. E., and Durisen, R. H. 1982, *Ap. J.*, **257**, 94.
van Albada, T. S., Kotanyi, C. G., and Schwarzschild, M. 1982, *M.N.R.A.S.*, **198**, 303.
van Breugel, W. J. M., Schilizzi, R. T., Hummel, E., and Kapahi, V. K. 1981, *Astr. Ap.*, **96**, 310.
Wilson, A. S., and Ulvestad, J. S. 1982, *Ap. J.*, **263**, 576.
Woltjer, L. 1972, *Ann. Rev. Astr. Ap.*, **10**, 129.
Young, P. J. 1976, *A.J.*, **81**, 807.

A. BOKSENBERG: Royal Greenwich Observatory, Herstmonceux Castle, Hailsham, East Sussex BN27 1RP, England

H. BUTCHER: Kapteyn Astronomical Institute, University of Groningen, Postbus 800, 9700 AV Groningen, The Netherlands

M.-H. DEMOULIN-ULRICH: European Southern Observatory, Karl-Schwarzschild-Strasse 2, 8046 Garching bei München, Federal Republic of Germany